Brain hematoma segmentation based on deep learning and data analysis

Hao Liu[1], *Yufeng* Yuan[2], *Yijia* Zeng[1], *Yuwei* Cai[1], *Ruiquan* Chen[1], *Chuankai* Xu[3], *Yi* Xie[3], and *Xiao* Peng[1,*]

[1]Center for Biomedical Optics and Photonics (CBOP) & College of Physics and Optoelectronic Engineering, Key Laboratory of Optoelectronic Devices and Systems, Shenzhen University, Shenzhen 518060, P. R. China
[2]School of Electronic Engineering and Intelligentization, Dongguan University of Technology, Dongguan, 523808, P. R. China
[3]Department of neurosurgery, Shenzhen Nanshan District Shekou People's Hospital, Shenzhen 518067, P. R. China

Abstract. Brain hemorrhage is a threatening disease with a yearly increasing incidence. Computed tomography (CT) is a common method of obtaining hematoma information and periodically monitoring changes of brain injuries. However, due to high frequency tomography, a large number of CT images is acquired, which complicates the analysis process. To increase the speed of analysis and ensure the accuracy of CT detection, we combined CT with deep learning to obtain automatic segmentation. In the present study, we developed a segmentation model based on a U-net with residual effects, for hemorrhage images. First, we screened the data and separated it into three parts for training, evaluation, and blind testing. Second, we pre-processed the dataset for data augmentation, which was used to avoid overfitting. After data augmentation, we transferred the data to an algorithm for training. As for the final model, we obtained an image segmenter with a mean intersection over union score of 0.8871 and dice score of 0.9362. The velocity of this algorithm was 26.31 fps, which greatly increased the speed of analysis. Thus, the segmenter obtained high detection efficiency and quantitative detection, which was suitable for periodically monitoring the areas of bleeding and assisting physicians in developing therapeutic regimens. Furthermore, the binary segmentation algorithm can be used for the development of pretraining models for classified segmentation tasks of CT images of head hemorrhages.

1 Introduction

As an important human organ, the brain is the most developed part of the nervous system, and is composed of left and right hemispheres, as well as connecting nerve fibers. The brain plays an important role in human movement, emotion, language, emotion, and physiological regulation, so a healthy brain is necessary for control of normal human behavior. It is assumed that when the brain is damaged, human activities are often greatly

* Corresponding author: pengxiao_px@szu.edu.cn

affected. Among brain injuries, intracerebral hemorrhage, a type of brain stroke injury, commonly occurs. It is usually caused by bursting of local blood vessels in the brain, resulting in a large amount of blood penetrating into the surrounding environment of brain cells. This affects human behavior by greatly disturbing the normal physiological activities of surrounding brain cells. According to recent data[1], from 1990 to 2019, the global number of stroke patients continuously grew every year. In 2019, the number of cases increased 70% relative to the number in 1990, when cerebral hemorrhages accounted for approximately 20% of the total number of stroke cases. Thus, it is a serious disorder threatening human health. In addition, intracerebral hemorrhage has a high early mortality, so it is important to make an early diagnosis and treat the disorder in its early stages. Neural imaging, including computed tomography (CT) and magnetic resonance imaging (MRI), are the most commonly used methods for detecting intracerebral hemorrhages. Using these methods, radiologists can visualize hemorrhages and make timely diagnoses. CT can clearly identify the bleeding site and hematoma size, with the ability to recognize acute intracerebral hemorrhages, while MRI has a better ability to detect lesions. Moreover, dynamic CT can also detect changes of intracerebral hemorrhages, which is important for diagnosis and continuous observation of treatment effects. However, because the type of tomography used affects the methods of detection, multiple scans can produce a copious amount of data, which presents challenges in data analyses. It is therefore important to simplify this process, but due to the complex structure of the brain, it is difficult for current image processing methods to extract the features of bleeding, which is not conducive to rapid detection.

In recent years, with the development of deep learning, feature extraction methods based on convolutional neural networks have widely used computer analyses. Multilayer convolution can effectively extract the features of images, to be used for future clinical decisions. For brain CT imaging, the convolution network can effectively extract structural features of the image and determine whether the case involves intracerebral hemorrhages. For classified tasks, previous studies[2,3] have achieved more than 0.9 accuracy. By changing the model structure to a full convolution model, we can classify images at the pixel level, so it is then possible to use image semantic segmentation. There have been several types of studies on brain CT segmentation, involving lesion segmentation[4,5] and issue segmentation[6]. Lesion segmentation is used to determine the loss of lesions between the baseline and the prediction of CT images. The main problem using this task involves sample imbalance, which is caused by the relatively small lesion object and large background. Based on these considerations, this study combined the residual block[7] with the U-net[8] to enhance the semantic connection and adjust the weight loss of the object to improve the detection of small objects. As a result, we developed a highly accurate model for semantic segmentation of hematomas, which should assist radiologists in diagnosing and continually monitoring treatment effects.

In the present study, we obtained a brain CT dataset according to Murtadha Hssayeni[9]. It contained 82 anonymous cases, of which 36 had symptoms with five types of intracerebral hemorrhages, including intraventricular, intraparenchymal, subarachnoid, epidural, and subdural hemorrhages. After data screening, we preprocessed the images and transferred them to a training model. After completion of the model, we blindly tested the model using some images that were not involved in model development. After debugging of several parameters, a final model with high accuracy was obtained.

2 Methods

2.1 Data screening

There were 82 cases in the dataset with approximately 30 images with a size of 650 × 650 per case. The total number of images was 2,501, with some counts of radiological labels. Regarding label imaging, there were only two kinds of grayscales, which mapped to the original CT image backgrounds, with objects identifying brain hematomas. Initially, we needed to resize the images to 512 × 512. We then screened 243 images with labels from the whole dataset as the segmentation dataset and classified it into three parts involving the training, testing, and validation sets. We finally obtained 194 images, with 25 images for evaluations and 24 images for validations.

2.2 Data augmentation

After data screening, the images needed to be converted, to match the algorithm and augment the universality of the data. The preprocessing method involved normalization, random flipping, random resizing, random cropping, and adding random noise[10]. First, we normalized the dataset, to normalize the grayscale to [-1, 1]. Second, we analyzed the training set by randomly cropping the center or randomly resizing by bilinear interpolation, with the results padded by zero, to the original size. Finally, we randomly flipped and added random noise.

2.3 Model training

We developed the detection model based on Res-Unet[7, 8] (Residual U-Net). Res-Unet is a full convolution neural network, combined with a residual convolution block. It was divided into two steps involving encoding and decoding. Encoding was constructed by two convolutions and a single pooling, and the residual effect was raised by adding the encoding results with down-sampling input, convoluted through a 3 × 3 kernel with a strike of 2. After three encoding blocks, a feature map of the original inputted images was obtained, as shown in Formula 1. For decoding, the feature map was treated with four decoding blocks, which contained two convolution layers involving one up-sampling layer and a residual result. The input of decoding blocks was then merged by outputting of encoding blocks with the same size. The output of the decoding process was a multi-dimensional tensor with size of $[n,512,512]$ as a pixel classified map, which was treated using a softmax classifier[11] on the first dimension to predict the type of each pixel. The softmax classifier is shown in Formula 2. To develop the model, the loss was calculated based on the pixel classified map and ground truth. In this process, we used the binary cross entropy (BCE) loss with a class weight to decrease the effect of sample imbalance, as shown in Formula 3.

$$g(i,j)=\sum_{k,l} f(i-k,j-l)h(k,l)+f(i,j) \tag{1}$$

$$P_i=\frac{e^{V_i}}{\sum_{i=1}^{n} e^{V_i}} \tag{2}$$

$$L=-\frac{1}{N}\sum_{i=1}^{N}[\alpha\cdot y_i\cdot\log(p_i)+\beta\cdot(1-y_i)\cdot\log(1-p_i)] \tag{3}$$

The parameters, α and β were the class weights of the object and background, respectively, the p_i was the probability calculated by the softmax classifier, and y_i was the ground truth. The class weights were used to increase the proportions of object losses. According to the mean loss per pixel, the weights of the model were updated using back propagation.

2.4 Evaluation and testing

When training, we evaluated the training results using testing sets per epoch. To obtain a high performance model, we adjusted our strategies according to the evaluations. After obtaining the best model, we validated it using a validation set.

3 Results and discussion

3.1 Evaluation

We evaluated the training results according to the accuracy, dice coefficient, and mean intersection over union (MIOU). The accuracy was defined as the ratio of the true case to the sum, as shown in Formula 4. The segmentation task was defined as the ratio of the true predicted area containing the background and object to the whole area. The MIOU was defined as the ratio of the true positive to positive and true negative, as shown in Formula 5. While in this task, it involved staggered areas of the predicted and true labels. The dice coefficient[12], used for evaluations in medical imaging segmentation tasks, was defined by Formula 6.

$$Acc=\frac{TP+TN}{N+P} \tag{4}$$

$$Miou=\frac{TP}{TP+FP+FN} \tag{5}$$

$$Dice=\frac{2TP}{2TP+FN+FP} \tag{6}$$

3.2 Experiment results

We divided the super parameter testing into two parts involving the basic learning rate and class weight of the BCE loss. For the basic learning rate, we set a learning rate strategy with five epoch linear warm-ups[13]. Based on the loss and accuracy, we adjusted the different basic learning rates to detect the convergence performance and selected a suitable basic learning rate.

As shown in Figure 1, the loss of declining speed and the accuracy of the rising speed performed in different situations. Compared to 0.0003 and 0.0001, the model converged quickly when the base learning rates were 0.001 and 0.0005. The learning rate also needed to be small when the model converged to the lowest point. To converge the model in high

speed and raise the probability of converging to the lowest point, we finally selected 0.0005 as the basic learning rate. We then adjusted the object class weight and the α value of the BCE loss, as shown in Formula 3, to reduce the negative effects brought by sample imbalance and to avoid model instability caused by excessive object loss of weight. Differing from the normal cross entropy with weight[14], we kept the weight of the background to retain stability and increase the weight of object losses, to allow the model to converge in the direction of the object loss reduction.

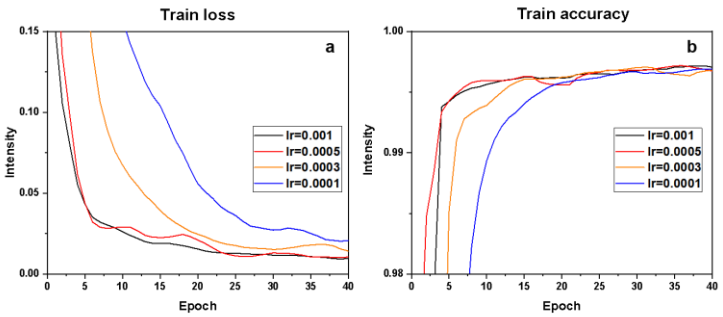

Fig. 1. The training results based on different learning rates. (a) The training loss curve based on different basic learning rates. (b) The training accuracy curve based on different basic learning rates.

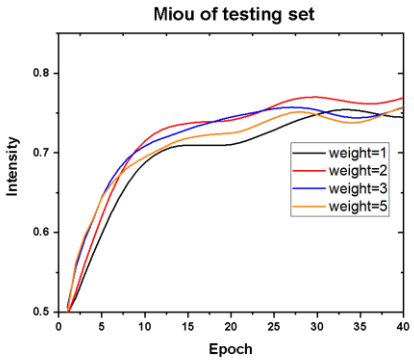

Fig. 2. The mean interaction over union (MIOU) of the testing set based on different object class weights of 1, 2, 3, and 5.

As shown in Figure 2, the mean MIOU evaluated in the testing set constantly increased by raising the epoch. When the weight was 2, the mean MIOU was higher than normal cases, which was the weight of 1 (black curve shown in Figure 2). Compared to a weight of 1, the weights of 3 and 5 improved the MIOU on the previous training stage. However, it became unstable after the 30th epoch because the excessive weight of the object loss made it difficult for the model to converge. When the loss of background declined, the reflection on the mean loss was much lower than the real decline, which was disadvantageous for updates of model parameters. We therefore selected the weight of 2 to conduct the development of 200 epochs, and saved the training model per 25 epochs to evaluate the model in the validation set.

When we obtained the segmentation model, we evaluated it using the segmentation validation set. Figure 3 shows that the total evaluation and we got a best model on the 200th epoch, which had a MIOU of 0.8871, dice coefficient of 0.9362, and process speed of 26.31 fps. Based on the best model, the predictive result of some validation set were shown in Figure 4.

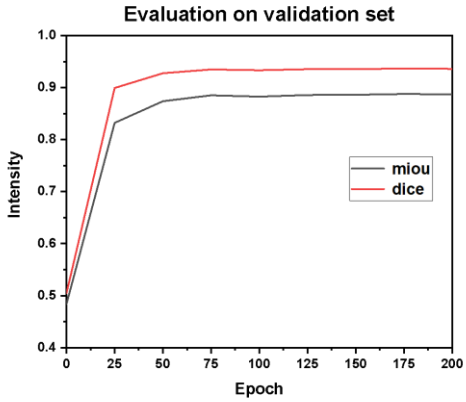

Fig. 3. Evaluation of the final training results in the validation set contained the mean intersection over union (MIOU) curve and the dice coefficient curve.

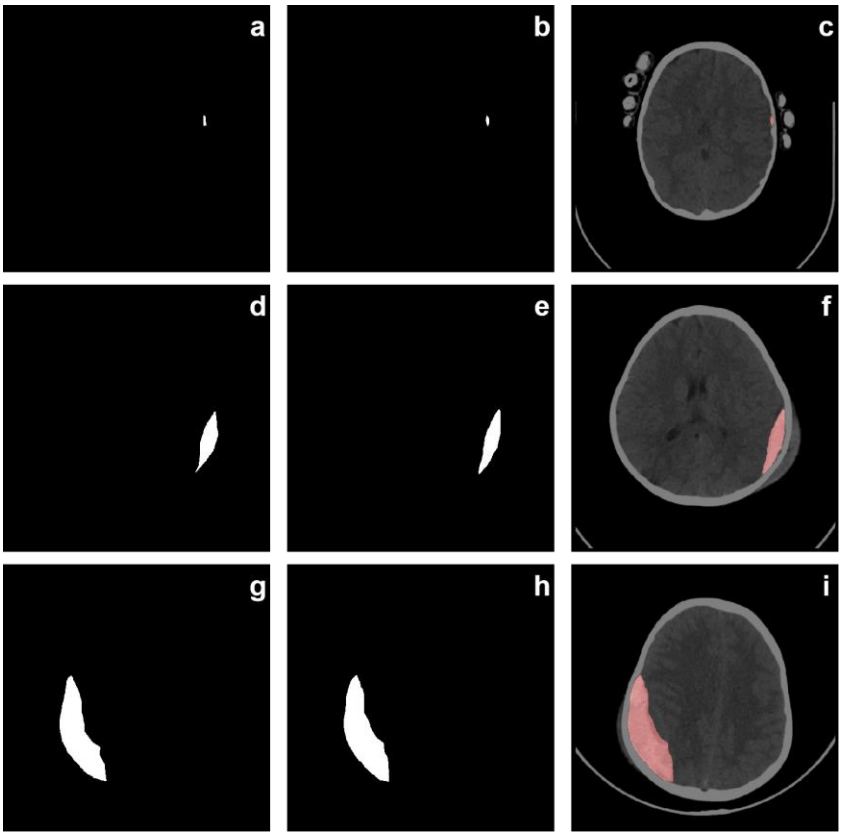

Fig. 4. The ground truth and output results of three samples involving small, medium, and large objects from the validation set. The (a, d, and g) are the ground truth from radiological labels of dataset, the (b, e, h) are the predictive results of the best model, and (c, f, i) are the blending results of the original images and predictive labels. Figure 4 shows that the final model performed well using a validation set for the detection of position and size. The shapes of the edges of the predictive label were smoother than the ground truth, which caused some false detection, especially on small objects, when compared with Figure 4(a) and 4(b).

4 Conclusions

The purpose of this work was to develop a highly efficient detection method of brain hemorrhages using CT. We used deep learning to obtain an automatic segmenter using data analysis. After adjusting development strategies, we obtained a brain CT segmenter based on Res-Unet, a fully convolution neural network combined with residual effects. After evaluations using a validation set, the MIOU of the final model was 0.8871 and the dice coefficient of the model was 0.9362. In addition to the evaluation of accuracy, this model had a processing speed of 26.31 fps. Furthermore, the output images of the validation set performed well when detecting the position and size of objects. However, there was some false detection caused by the smooth edges of the output.

Although there were a small false detection rate, with high accuracy and a high MIOU, this algorithm model was useful for the analysis of segmented hematoma areas and quantitative analyses of lesion areas, which is of great significance for developing a therapeutic schedule. Furthermore, the segmentation model could be secondarily used to classify hemorrhage types using new datasets, or further developed by using a new dataset to achieve higher accuracy and robustness.

This work has been partially supported by the National Natural Science Foundation of China (31771584/62075137), the Guangdong Basic and Applied Basic Research Foundation (2020A1515010377) and the Science Foundation of Shenzhen University (Grant No. 2017000193).

References

1. V. L. Feigin, B. A. Stark, C. O. Johnson, et al. Global, regional, and national burden of stroke and its risk factors, 1990–2019: a systematic analysis for the Global Burden of Disease Study 2019[J]. The Lancet Neurology, **20**(10):795–820(2021).
2. H. Abdulkader, E. F. Georges, S. Hadi, U. O. Dilber. Deep networks in identifying CT brain hemorrhage. Journal of Intelligent & Fuzzy Systems, **35**(2):2215–2228(2018).
3. A. D. Muhammad, Y. Kamil, O. Huseyin. Application of Deep Learning in Neuroradiology: Brain Haemorrhage Classification Using Transfer Learning. Computational Intelligence and Neuroscience, **2019**:1-12.
4. A. Motahareh, A. Ali, E. Mehdi. Brain tumor image segmentation via asymmetric/symmetric UNet based on two-pathway-residual blocks. Biomedical Signal Processing and Control, **69**:102841(2021).
5. L. Li, M. Wei, B. Liu, K. Atchaneeyasakul, F. Zhou, Z. Pan, S. Kumar, J. Zhang, Y. Pu, D. Liebeskind, F. Scalzo. Deep Learning for Hemorrhagic Lesion Detection and Segmentation on Brain CT Images. IEEE journal of biomedical and health informatics, **25**(5):1646 - 1659(2021).
6. F. Liu, H. Jang, R. Kijowski, T. Bradshaw, A. B. McMillan. Deep Learning MR Imaging–based Attenuation Correction for PET/MR Imaging. Radiology, **286**:2(2017).
7. K. He, X. Zhang, S. Ren, J. Sun. Deep Residual Learning for Image Recognition. 2016 IEEE Conference on Computer Vision and Pattern Recognition (CVPR), **2016**:770-778.
8. O. Ronneberger, P. Fischer, T. Brox. U-Net: Convolutional Networks for Biomedical Image Segmentation. Lecture Notes in Computer Science. **9351**:234-241(2015).
9. M. Hssayeni, M. Al-Janabi, A. D. Salman, H. F. Al-khafaji, Z. A. Yahya, B. Ghoraani. Intracranial Hemorrhage Segmentation Using A Deep Convolutional Model. Data, **5**(1):14(2020).

10. P. Chlap, M. Hang, N. Vandenberg, J. Dowling, L. Holloway, A. Haworth. A review of medical image data augmentation techniques for deep learning applications. Journal of Medical Imaging and Radiation Oncology, **65**:545-563(2021).
11. A. Krizhevsky, I. Sutskever, G. Hinton. ImageNet Classification with Deep Convolutional Neural Networks. Communications of the ACM, **60**(6):84-90(2017).
12. D. G. Shen, G. R. Wu, H. Suk. Deep Learning in Medical Image Analysis. Annual Review of Biomedical Engineering, **19**:221-248(2017).
13. E. Kim, K. H. Lee, W. K. Sung. Optimizing Spatial Shift Point-Wise Quantization. IEEE Access, **9**:68008-68016(2021).
14. Z. S. Xu, M. M. Xia. Hesitant fuzzy entropy and cross-entropy and their use in multiattribute decision-making. International Journal of Intelligent Systems, **27**(9):799-822(2012).